9724 *Macromolecules* **2010**, *43*, 9724–9735
DOI: 10.1021/ma101868y

Macromolecules
ARTICLE

Surface Plasmon Resonance (SPR) Detection of Theophylline via Electropolymerized Molecularly Imprinted Polythiophenes

Roderick B. Pernites, Ramakrishna R. Ponnapati, and Rigoberto C. Advincula*

Department of Chemistry and Department of Chemical and Biomolecular Engineering, University of Houston, Houston, Texas 77204-5003, United States

Received August 14, 2010; Revised Manuscript Received October 26, 2010

ABSTRACT: A facile approach to tailor-made, highly selective, and robust ultrathin sensor film for theophylline detection was demonstrated by an electropolymerized molecularly imprinted polymer (E-MIP) film of a terthiophene derivative. The method involved direct electropolymerization of the H-bond complexing terthiophene monomer. A key enabling step in sensor fabrication is the use of an electrochemically mediated washing step of the template. The formation of the E-MIP film was monitored by *in situ* electrochemical surface plasmon resonance (EC-SPR) spectroscopy, allowing real-time observation of the simultaneous changes in electrochemical and optical properties of the film. Surface characterization techniques for the electropolymerized films include atomic force microscopy (AFM), ellipsometry, static contact angle, X-ray photoelectron spectroscopy (XPS), and quartz crystal microbalance (QCM). A linear calibration curve ($R = 0.994$) of the E-MIP/SPR sensor for theophylline detection was obtained with a $10-50\,\mu M^{-1}$ range and a limit of detection (LOD) of $3.36\,\mu M^{-1}$. The fabricated E-MIP sensor film showed a homogeneous surface coverage, high sensitivity, long-term stability, and strong selectivity toward the imprinted template molecule. This indicated the formation of precise and stable cavities that retained the exact memory of the size, shape, and orientation of the functional groups during the templating electropolymerization steps.

Introduction

Theophylline, one of the most clinically monitored drugs, is frequently used as bronchodilators and respiratory stimulators for the treatment of the symptoms of acute and chronic asthmatic condition. However, an overdose of theophylline can be lethal or lead to permanent neurological damage.[1] The safe and effective use of this drug molecule relies on careful dosage adjustments based on accurate measurements of theophylline concentration in the blood serum. Theophylline with theobromine and caffeine (and other xanthine derivatives) can also be found in food products such as tea, coffee, cocoa beans, and chocolates. These compounds, which have been reported by the National Institute of Standards and Technology (NIST), have received increased attention in the food and nutrition industry for their various physiological effects.[2] It is necessary and important to cautiously analyze food products that might have an excess amount of these xanthine classes of compounds. Thus, convenient and reliable methods for detection and rapid online analysis of theophylline are of high importance.

The ideal measurement system of theophylline should be sensitive, selective, robust, and relatively inexpensive. The molecular imprinted polymer (MIP) technique has been demonstrated as one of the most promising techniques in sensor technology because of its simplicity, reliability, capability of miniaturization, and low cost method of fabrication. Generally, the imprinting procedure involves polymerizing functionalized monomers with cross-linkers in the presence of the template molecule (analyte). The subsequent solvent extraction of the template from the polymer film creates complementary cavities (also called imprint sites) that contain the memory of the size, shape, and functional group orientation of the imprinted molecule. As a result, the polymer film serves as a selective recognition element or artificial receptor for the rebinding of the template.

A noncovalent MIP approach[3] involves a template that is not covalently bound to the monomer. It relies mainly on weak intermolecular interactions resulting from electrostatic attractions, hydrophobic interactions, H-bonding, $\pi-\pi$ stacking, metal coordination, charge transfer, etc. Most MIP films are prepared using this approach because of its simplicity of fabrication, commercial availability of functional monomers that are capable of hydrophobic interactions and H-bonding, and ease of removal of the template molecule by simple washing even with a mild solvent condition. The idea of noncovalent MIP using organic polymers was first introduced by Mosbach in the 1980s.[3] Since then, a large number of studies have been reported to detect a variety of analytes using noncovalent MIP.[4]

Surface plasmon resonance (SPR) sensing of theophylline was performed using the MIP film prepared by *in situ* electrochemical polymerization. SPR is a well-established, noninvasive, and surface-sensitive analytical technique capable of providing information about interfacial phenomena. SPR spectroscopy measures the optical dielectric constants of thin films deposited onto noble-metal-coated substrates. Recently, label-free sensors based on imprinted thin films on SPR chips have been reported.[5] Rapid, label-free, high-sensitivity, and real-time measurements are the hallmarks of SPR for sensing. In general, sensing occurs when light is coupled to a metal under total internal reflection conditions. In the presence of an external event on a dielectric layer, the refractive index and the thickness of the sensor surface change upon binding of the target analyte to the surface. SPR have also been proven to be highly sensitive for monitoring changes at the electrode and electrolyte solution interface.[6] For example, the technique has been successfully demonstrated by our group in

*Corresponding author: e-mail radvincula@uh.edu; Ph +1 713 743 1760.

 Published on Web 11/16/2010

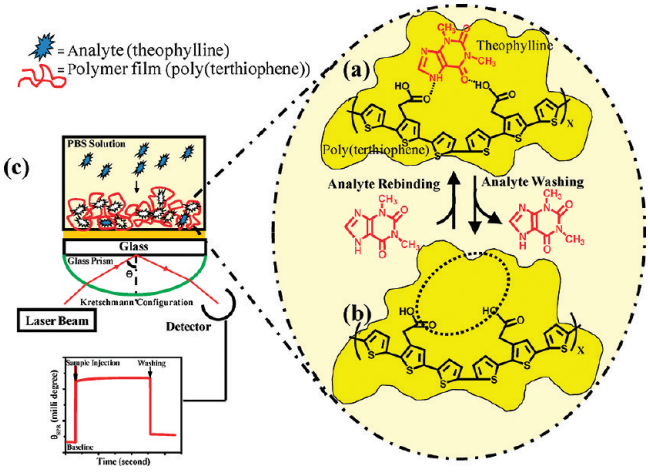

Figure 1. (a) Molecular imprinting of the template. (b) Formation of cavity after washing the template. (c) SPR setup for sensing of the template.

sensing various analytes[7] including a nerve agent analogue.[8] More detailed information about the principles of SPR measurements can be found elsewhere.[9] The combination of SPR with electrochemical measurements or EC-SPR is a powerful analytical technique for the simultaneous characterization and manipulation of electrode|electrolyte interfaces.[7,8] An advantage of using the EC-SPR technique is that the electrochemical and optical properties are simultaneously obtained on surfaces and ultrathin films at the nanometer scale. It has been employed to monitor the interfacial reactions and the buildup of complex architectures at solid−liquid interfaces.[10] In EC-SPR, the Au substrate which carries the optical surface mode is also used as the working electrode for electrochemical/potential experiments. In the past, our group has shown the use of SPR, EC-SPR, and AFM-EC-SPR in characterizing the formation of ultrathin films of conducting polymers on gold substrates.[11] The latter involved the simultaneous monitoring with an atomic force microscope (AFM).

In this paper, the sensing of theophylline by SPR utilizing ultrathin films of electrochemically molecularly imprinted polymer (E-MIP) films of the carboxyl functionalized-terthiophene monomer is reported (Figure 1). This monomer has several advantages compared to direct electropolymerization of thiophene. These include noncovalent binding with the analyte, lower oxidation potential, and cross-linkability. To the best of our knowledge, the use of poly(terthiopene) as a conducting polymer for imprinting and sensing of theophylline has not been previously reported. It should be noted also that its advantage in template removal or sensor regeneration has not been carefully explored. The imprinting of theophylline was achieved previously by electropolymerization of either phenol or methylene green[12] as functional monomers. Unlike most MIPs, our method employs the complexing ability of a single monomer to the template via the orthogonal −COOH functional group and also facilitates cross-linking through the terthiophene pendant group. The terthiophene units are then free to polymerize both in an intra- and intercomplex manner more similar to a cross-linking process. Thus, the use of a π-conjugated poly(terthiophene) presented the proper combination of electropolymerizability, stability, and doping (swelling) properties that enabled the demonstration of an improved sensitivity, high selectivity, and robust chemical sensing. In addition, an efficient and faster method of template removal employing the electrochemical properties of the poly(terthiophene) matrix has been developed. This has led to better sensitivity and selectivity for analyte detection. Moreover, we demonstrate the robust characteristics of this chemical recognition element through several cycles of sensing (i.e., 45 days) with only 15% attenuation.

Scheme 1. Synthesis Route of 2-(2,5-Di(thiophen-2-yl)thiophen-3-yl)acetic Acid (G0-3T COOH)

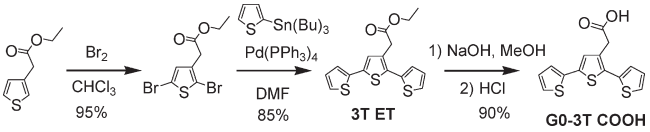

Experimental Section

Materials. The chemicals used were purchased from Sigma-Aldrich except for the terthiophene monomer with carboxylic acid functional group (2-(2,5-di(thiophen-2-yl)thiophen-3-yl)acetic acid abbreviated as G0-3T COOH), which was synthesized by a modified procedure reported previously (Scheme 1).[13] The details of the synthesis and their NMR spectra (Figures 1−3) are found in the Supporting Information. A monomer-to-template ratio of 2:1 molar ratio was used in making the MIP film. This optimum ratio was determined from the theoretical modeling studies, which is later discussed. For instance, the MIP solution was prepared by mixing 200 μM of G0-3T COOH (monomer) with 100 μM theophylline (template) in acetonitrile (ACN) with 0.1 M tetrabutylammonium hexafluorophosphate (TBAH) or 0.1 M lithium perchlorate ($LiClO_4$). The nonimprinted polymer (NIP) solution was prepared in the same manner but without the addition of the template. For sensing experiments, the solutions of theophylline and the other analytes were prepared in 0.1 M PBS (phosphate buffered saline) solution at different concentrations. The MIP solution was prepared at least 24 h prior to the electropolymerization to allow complexation of the monomer and template in solution (called prepolymerization complex).[14]

Gold-coated (ca. 50 nm) BK 7 glass slide or silicon wafer was used for all electropolymerization and optimization studies in an *ex-situ* setup. Electropolymerization of the MIP and NIP films for XPS measurements was performed onto gold-coated BK7 glass slide or silicon wafer. The gold coating was deposited onto the BK7 glass substrates or silicon wafer with 2−5 nm thick chromium adhesion layer by thermal evaporation (Edwards E306) at a rate of 1.0−1.2 Å s^{-1} operating under high vacuum (10^{-6} bar). For *in situ* electropolymerization and SPR sensing, the gold substrate (50 nm) with titanium interface (1.5 nm) was provided by Brinkmann Instruments (now Metro Ohm USA) and Eco Chemie. Prior to electropolymerization, the evaporated and commercially available gold substrates were subjected to oxygen plasma cleaning (Plasmod, March Instruments) for 120 s.

EC-SPR Electropolymerization and SPR Sensing. All electropolymerizations were performed in an Autolab PGSTAT 12 potentiostat (Brinkmann Instruments) coupled with an SPR instrument (Autolab ESPRIT from Eco Chemie). The Autolab SPR setup is based on a Kretschmann configuration with a 670 nm laser source. The gold substrate, which served as the surface plasmon resonator, was also used as the working electrode for the electrochemistry setup in a standard three-electrode measuring cell with platinum rod as the counter electrode and Ag/AgCl wire as the reference electrode (inserted at the top of the sample channel). The potentiostat and SPR instruments were controlled using GPES version 4.9 and ESPRIT version 4 programs. Both softwares were provided by Metro Ohm and Eco Chemie. The electropolymerization was performed using the cyclic voltammetry technique (CV) by sweeping the voltage from 0 to 0.8 V for 20 cycles at a scan rate of 50 mV/s. For *ex-situ* setup (not coupled to SPR instrument), the electropolymerization was performed using the evaporated gold substrate inserted onto a fabricated electrochemical cell (Teflon made) with a diameter of 1.0 cm and volume of 0.785 cm^3. Prior to sensing, the stabilization of the electropolymerized films were completed by injecting 50 μL of PBS buffer onto the substrate several times until a stable SPR response is achieved. During sensing, the Autolab SPR was set to automated injection of the background solution (PBS buffer) for 120 s followed by sample

injection (50 μL volume) for 900 s and then rinsing of the film with the background solution for 300 s. The SPR response due to the binding of the template and other analytes only were compared and plotted after the abrupt change in angle, which is mainly due to the change in the refractive index of the bulk solution. All the SPR angular and kinetic curves were normalized to zero. Curve and peak analysis were done using Origin Lab version 7.

QCM Measurements. The fabrication of the MIP film using *in situ* electropolymerization was also monitored by quartz crystal microbalance (QCM) coupled to an electrochemistry setup with the same standard three-electrode system. The QCM apparatus, probe, and crystals were made available from Maxtek Inc. (Inficon). The AT-cut polished QCM crystals (5 MHz) with 13 mm diameter was used as the working electrode. The data acquisition was done with an R-QCM system equipped with a built-in phase lock oscillator and the R-QCM Data-Log software. The QCM crystals were cleaned with an oxygen plasma etcher (Plasmod, March) immediately prior to use. The resulting change in frequency can be used to calculate the mass change due to the adsorbed material onto the film using the Sauerbrey equation:[15]

$$\Delta F = \frac{-2F_q^2 \Delta m}{A\sqrt{\rho_q \mu_q}} \quad (1)$$

where ΔF is the change in frequency, Δm is the mass change, F_q (= 5 MHz) is the resonant frequency of the QCM crystal, A (= 1.227 cm^2) is the area of the electrode, ρ_q (= 2.65 g/cm^3) is the density of the quartz, and μ_q (= 2.95 $\times$ 10^6 N/cm^2) is the shear modulus of the quartz.

Ellipsometry Measurements. The thickness of the electropolymerized film was measured by ellipsometry using the Multiskop ellipsometer (Optrel GmbH, Germany) equipped with a 632.8 nm laser. The measurements were all done at 60° angle of incidence with respect to the surface normal under dry and ambient conditions. Several measurements were performed for each film at various positions. The measured values of delta and psi were used to calculate the thickness of the film using an integrated specialized software (Elli, Optrel) that was provided with the instrument.

Water Contact Angle Measurements. The static contact angle of the electropolymerized film was measured using a CAM 200 optical contact angle meter (KSV Instruments Ltd.) with CAM 200 software. The measurement was achieved by making approximately a 1 μL drop of Milli-Q water onto the film. Several measurements were also performed for each film at various positions.

AFM Measurements. Atomic force microscopy (AFM) with an Agilent 5500 AFM/SPM System (Agilent Technologies) was used to investigate surface morphologies of the electropolymerized film. The AFM measurements were carried out using a piezo scanner capable of scanning an area of ~10 $\times$ 10 μm^2 at room temperature. The scanning rate was 0.8−1.0 lines/s. Commercially available tapping mode tips (TAP300, Silicon AFM Probes, Ted Pella, Inc.) were used on cantilevers with a resonance frequency in the range of 290−410 kHz. For AFM scanning under ambient and dry conditions, all electropolymerized films were rinsed thoroughly with solvent and carefully dried under nitrogen gas. All AFM topographic images (MAC and tapping mode) were filtered and analyzed by using SPIP software (Scanning Probe Image Processor, Imagemet.com).

XPS Measurements. A PHI 5700 X-ray photoelectron spectrometer was equipped with a monochromatic Al Kα X-ray source ($h\nu$ = 1486.7 eV) incident at 90° relative to the axis of a hemispherical energy analyzer. The spectrometer was operated both at high and low resolutions with pass energies of 23.5 and 187.85 eV, respectively, a photoelectron takeoff angle of 45° from the surface, and an analyzer spot diameter of 1.1 mm. The survey spectra were collected from 0 to 1400 eV, and the high-resolution spectra were obtained for C 1s, O 1s, S 2p, S 2s, Au 4f, and N 1s. All spectra were collected at room temperature with a base pressure of 1 $\times$ 10^{-8}. Electron binding energies were calibrated with respect to the Au 4f$_{7/2}$ peak at 84.0 eV.[16] The peaks were analyzed first by background subtraction using the Shirley routine. The binding energies for each peak were assigned based on published literature values. All the samples (electropolymerized film on gold-evaporated silicon wafer or BK 7 glass) were completely dried in argon gas prior to XPS measurements.

Results and Discussion

Theoretical Modeling of the Monomer−Template Complex in Solution (Prepolymerization). The MIP sensor film was prepared by electropolymerizing 2-(2,5-di(thiophen-2-yl)thiophen-3-yl) acetic acid (G0-3T COOH) with theophylline in a 2:1 molar ratio, respectively. This ratio was deemed optimum based on the H-bonding site in a donor−acceptor pair as determined by modeling. The complexation between the monomer and template was modeled using Spartan '08 (V1.2.0), Wave function Inc. (AM1 semiempirical calculation), and the net binding energy (ΔE_f) of the monomer−template complex was achieved from the calculated enthalpies of formation (ΔH_f) using the formula

$$\Delta E_f = (\Delta H_{f,monomer-template}) - (\Delta H_{f,\,monomer} + \Delta H_{f,\,template}) \quad (2)$$

The same modeling and procedure have been applied to calculate for the interaction energy of other monomers and templates prior to polymerization to form an MIP.[17] The net binding energy of the complex with 2:1 momomer-to-template ratio was determined to be −104.731 kJ/mol, which indicates an energetically favorable complexation. The ΔE_f values of the other ratios were also calculated by using the same method, and the results are as follows: −23.678 and −3.965 kJ/mol for 1:1 and 3:1 ratio, respectively (2D computer generated images in Figure 4 of the Supporting Information). The 2:1 ratio showed the most negative energy of formation, signifying that a relatively stable prepolymerization complex is formed between theophylline and G0-3T COOH. The geometry-optimized structure is shown in Figure 2 where the theophylline is surrounded by the monomers. In this model, a desired cross-linkable conformation of the complex is evident which is necessary for robust and effective imprinting of the template molecule. Furthermore, the extent of H-bonding interaction between monomer and template was also determined. From the Spartan calculation, the 2:1 ratio displays a more stable complexation with higher probability of forming H-bonding between monomer and template. Clearly, the H-bonding (represented in broken lines) was formed between the oxygen atom of the theophylline and the OH functional group of the monomer (G0-3T COOH), and the H-bond distance is calculated to be ~2.094 Å. For other ratios, H-bonding is not very evident. Thus, the 2:1 ratio was used for the MIP electropolymerization.

Surface Imprinting of Theophylline by EC-SPR Monitoring. The CV electrodeposition was monitored *in situ* by the hyphenated EC-SPR technique, allowing the direct interfacing of the imprinted polymer film onto an electrode optical transducer surface (SPR Au substrate). The same *in situ* measurements were performed during the fabrication of the nonimprinted polymer (NIP) control film by electropolymerization. Figure 3a shows the SPR kinetic measurement during potential cycling (from 0 to 0.8 V and reverse) while Figure 3b depicts the potential ramp over time. A recurring oscillation is observed for each CV cycle that involved an oxidation followed by a reduction process. In Figure 3a, the

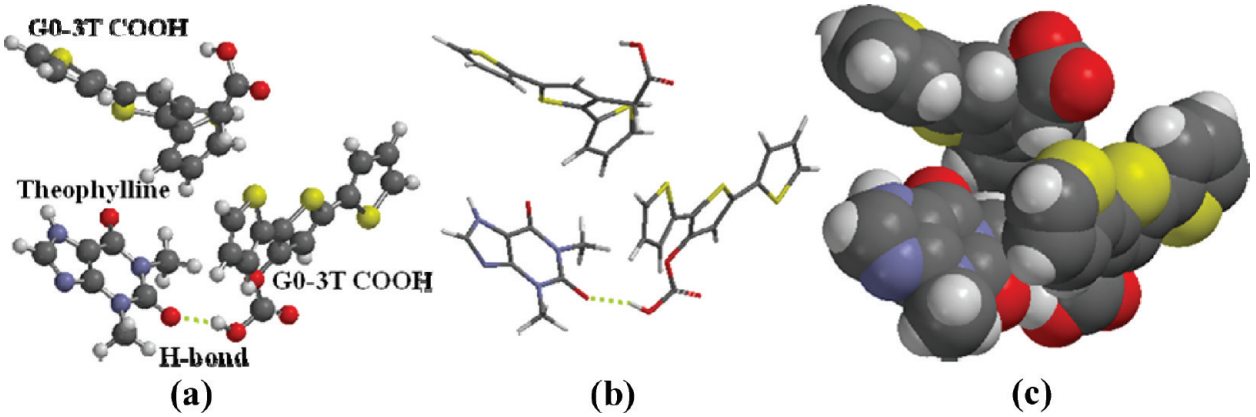

Figure 2. Computer-generated images of the 2D optimized structures (ball and spoke (a), tube (b), and space filling (c) models) of the prepolymerization complex between monomer and template (Spartan, Wavefunction Inc., semiempirical AM1 quantum calculations). Note color representation of elements: carbon (gray), hydrogen (white), nitrogen (blue), oxygen (red), and sulfur (yellow).

angle increased instantaneously at the start of the anodic scan (oxidation) and slightly decreased at the beginning of the cathodic scan (reduction). The profile achieved in the kinetic curve (Figure 3a) concurs with our earlier results on electropolymerization of conducting polymers, where the SPR response increases during oxidation and decreases upon reduction.[11c,e] This sequential oscillation is due to the changes in the dielectric property (related to the optical constants) of the poly(terthiophene) as it switches from oxidized (doped) to reduced (dedoped) states. The change in the optical property of the film is clearly seen in Figure 3a, where the SPR angle changes upon oxidation−reduction. A conducting material like poly(terthiophene) is characterized by a complex dielectric function[18] as it undergoes the doping/dedoping process:

$$\varepsilon = \varepsilon_{\text{real}} + \varepsilon_{\text{imaginary}} \tag{3}$$

where $\varepsilon_{\text{imaginary}} = (2\sigma\lambda/c)$, σ is conductivity, λ is wavelength of incident light, and c is the speed of light. From the equation, the variation of conductivity of the polymer film changes the imaginary part of the dielectric constant, resulting in changes in the optical constant manifested in the oscillation of the SPR kinetics during the cyclic potential growth of the polymer film.

The film formation was observed by an increasing SPR angle in the *in situ* kinetic measurement (Figure 3a) and SPR angle response versus the scanning potential (Figure 3c) during the whole process of polymerization. The SPR angular scan (inset of Figure 3a) taken before and after the electropolymerization process confirmed the result of the kinetic measurement. What is of interest is that the trend in reflectivity increase is linear and the sinusoidal behavior of the oscillation is nearly constant. This indicates a well-behaved film that is constantly coupled to the SPR resonance despite the changes in the dielectric properties with thicker films. A similar kinetic profile was observed during the NIP film fabrication by *in situ* electropolymerization (Figure 5 in the Supporting Information). It was evident from SPR kinetic measurements that the angular shift response value is higher during E-MIP film fabrication (angular shift ~800 mdeg) than the NIP (~510 mdeg), indicating that more materials were deposited during MIP film fabrication. This observation is also consistent with the QCM measurements, which shows more mass adsorbed with the MIP than the NIP (see Table 1 in the Supporting Information). It is possible that the effective complexation of the monomer and template makes the monomer more easily oxidized to form the ultrathin polymer film on the substrate. Further investigation about the kinetics of the film deposition is beyond the scope of the present paper.

The formation of the E-MIP film was also confirmed in the CV scan (Figure 3c, left *y*-axis) by an increasing current in the oxidation peak regime (~0.6−0.8 V), demonstrating an increase in conductivity of the substrate as a result of the deposition of the conducting polymer film. The increase in current during the anodic scan is accompanied by an increase in the SPR angle particularly at the onset potential of 0.6 V, except for the first CV cycle that immediately rise at 0.2 V (Figure 3c, right *y*-axis). As earlier reported,[11b,c,13] the increase in the SPR angle upon sweeping the potential is attributed to the changes in optical dielectric properties and thickness combined due to the electrodeposition of the conducting polymer film onto the Au substrate. Then the SPR angle faintly decrease (ca. 0.3 V in Figure 3c, right *y*-axis) during the reversal scan, which is attributed to the slight shrinking of the film as a result of releasing the counterions back into the bulk solution.[19] Note that the SPR angle did not return to its initial value, but rather it continues to augment until the last CV cycle that is similar to Figure 3a. During the potential growth of the polymer film, the peak potentials remained constant with increasing number of cycles (Figure 3c, left *y*-axis). This illustrates the stability of the redox property of the film regardless of the changes in both the thickness and the dielectric properties. Moreover, the same CV curve (inset of Figure 3c) was observed with the E-MIP film after scanning in the solvent containing only the supporting electrolyte (monomer-free scan or postpolymerization CV). This measurement was performed when the substrate was rinsed thoroughly with the solvent to remove excess monomer after completion of the electropolymerization process. Comparing the CV curve of the E-MIP with the NIP, no additional peak was observed within the scanned window, indicating that the template has no contribution to the electrochemical oxidation of the monomer. In addition, a separate study was performed to determine the electrochemical stability of the template by scanning the potential from 0 to 1.1 V. The results showed that an oxidation peak was formed in the anodic scan beyond 0.8 V, but further investigation was not performed on these findings. Hence, the sensor film was typically prepared by scanning up to 0.8 V in order to avoid any complications arising from possible electrochemical activity of the template.

The E-MIP film fabrication was also characterized by the QCM technique, which is a highly sensitive measurement for observing mass changes as a thin layer of material is adsorbed onto the quartz crystal. This technique has been used extensively by our group to study the *in situ* formation of a conducting polymer on Au QCM crystal.[11e,13,20] In QCM

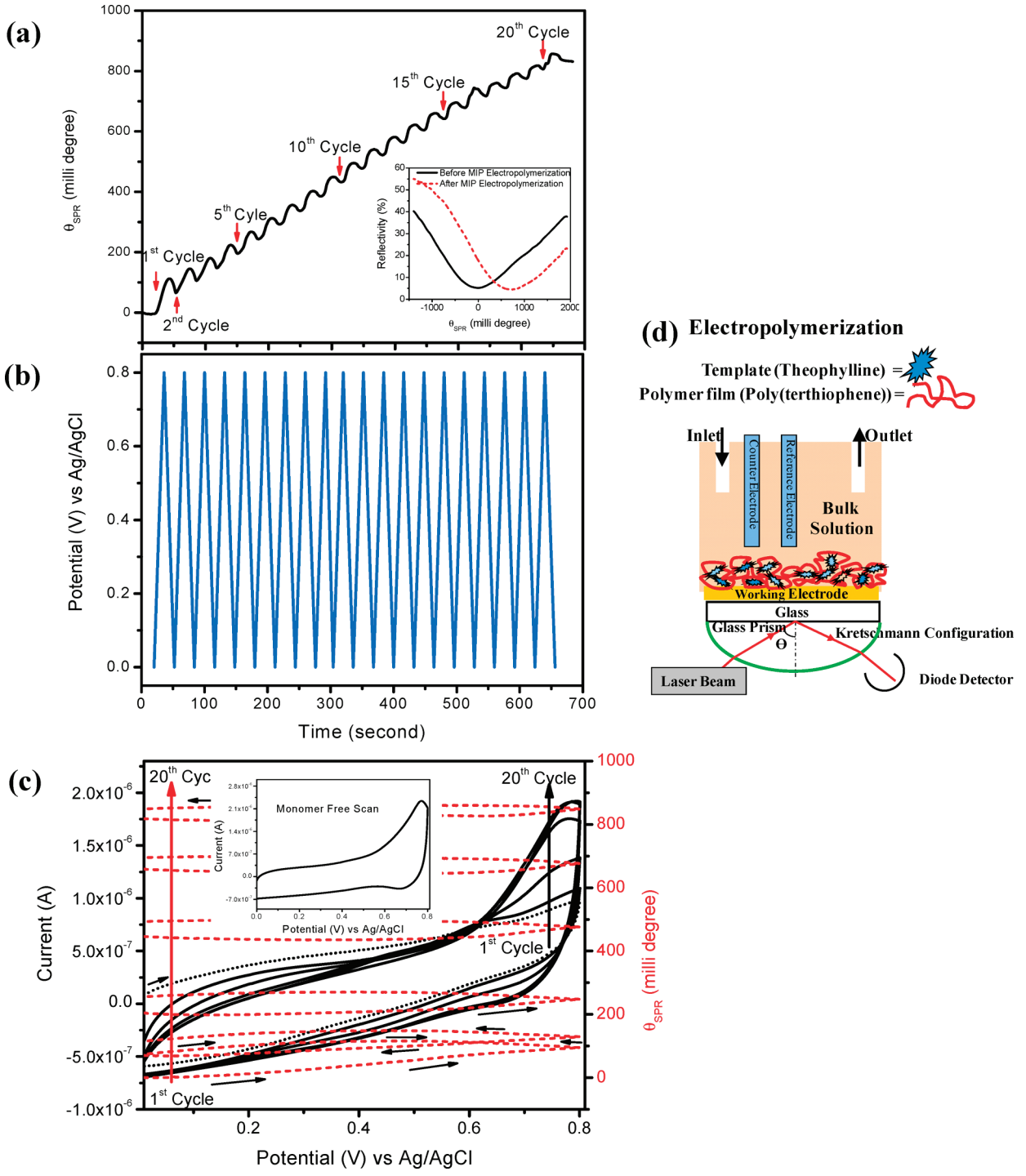

Figure 3. EC-SPR results during MIP film (200 μM G0-3TCOOH and 100 μM theophylline) formation: (a) SPR kinetic curve with SPR angular curve (inset) before and after electropolymerization, (b) potential ramp versus time, and (c) SPR angular scan (broken lines) and current response versus the scanning potential with inset of the monomer-free scan (representative CV cycles 1, 2, 5, 10, 15, and 20). (d) EC-SPR setup of *in situ* electropolymerization.

analysis, the amount of material deposited was determined using the Sauerbrey equation[15] from the frequency measurement of the QCM crystal before and after electropolymerization in air. With this condition, the viscous losses or viscoelastic effect can be neglected, which is not accounted for in the Sauerbrey approximation.[11e] Using the Sauerbrey equation, the absolute mass per unit area was calculated from the change in frequency (ΔF) due to the deposition of the polymer film. The amount of material deposited during E-MIP and NIP film fabrication was determined to be 1.20 and 0.62 μg cm^{-2}, respectively. The calculated densities of the films (see Table 1 in Supporting Information) were comparable to the reported density of the melamine-imprinted polymer film electropolymerized using a bis(bithiophene) derivative.[21]

Characterization of the Fabricated E-MIP and NIP Films. Additional surface-sensitive techniques were utilized to characterize the E-MIP and NIP films after fabrication by electrochemical polymerization. The use of different techniques to carefully analyze the E-MIP film before and after

template removal is seldom performed in most MIP studies. The results of the ellipsometry, contact angle, and AFM measurements are summarized in Table 1.

Figure 4 shows the AFM analysis of the films. Although the AFM image cannot be used to directly verify that theophylline is indeed imprinted onto the polymer film, important informations such as topography, porosity, and surface roughness of the films can be determined by the technique. The NIP film is analyzed first by AFM. Its topography and line profile scans were closer to the MIP film before constant potential washing. The AFM image of the NIP film showed good surface coverage and homogeneity for a conducting polymer film. The AFM results validate the earlier morphology studies of poly(thiophene) films that is characterized by high surface coverage and good homogeneity.[22] The use of terthiophene as functional and cross-linking monomer is advantageous because it can achieve a more ordered polymer structure as a result of the regular α, α-coupling (2,5 position) of the monomer units, resulting in more conjugated linear polymer segments.[23] In the case of monothiophene, α,β-coupling (2,4 position) can also take place during the polymerization,[24] hence resulting in a more disordered covalent connectivity (lower conjugation) and rougher surface polymer film. However, in terms of cross-linkability, the terthiophene monomer has an advantage in that both α positions of the terminal thiophene rings have a lower oxidation potential.

Table 1. Surface Characterization Measurements of the Three Electropolymerized Films in Figure 3

film	water contact angle (deg)	ellipsometry thickness (nm)	AFM rms (nm)
(a) NIP	55.84 ± 0.47	8.57 ± 0.28	1.15 ± 0.03
(b) MIP before template washing	56.20 ± 0.56	11.87 ± 0.26	1.11 ± 0.03
(c) MIP after template washing	52.45 ± 1.22	10.73 ± 0.23	1.60 ± 0.02

The H-bonding[25] ability of the orthogonal −COOH group[3b,26] of terthiophene enables anchoring of theophylline units in the middle while the electroactive group is intended for cross-linking with another monomer inter- or intracomplex to form a type of conjugated polymer network (CPN). Note that two or more monomers units present in the complex, possibly surrounding the template, should enable cross-linking polymerization as a matrix for MIP. The minimum requirement for cross-linking is a functionality or $f = 3$, whereas the 2:1 complex will have $f = 4$. This was confirmed by the theoretical modeling studies (Figure 2).

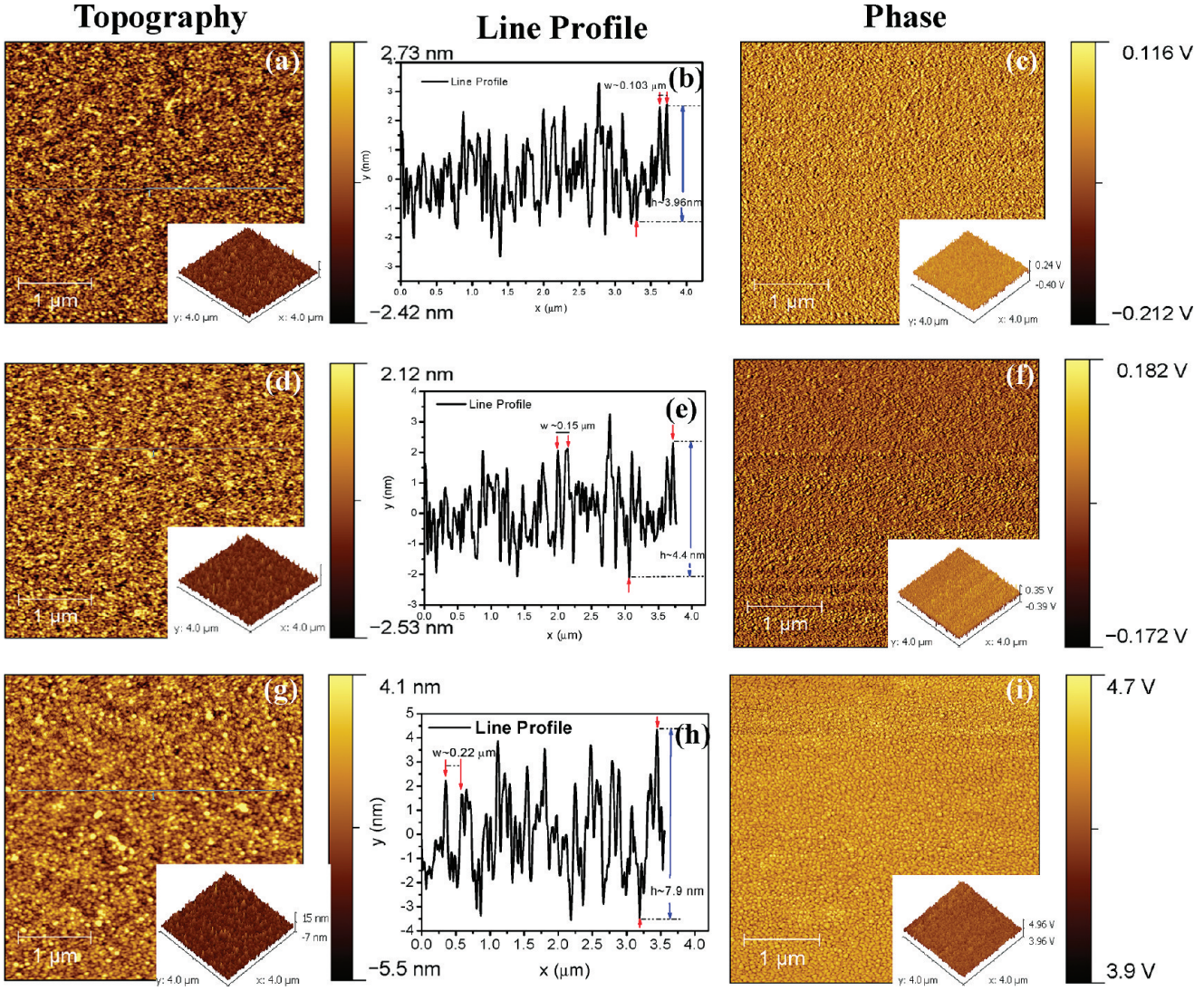

Figure 4. AFM analysis of the NIP (a, b, c), MIP before (d, e, f) and after (g, h, i) potential-induced washing: topography 2D images with 3D inset (a, d, g), line profiles of the topography images (b, e, h), and phase 2D images with 3D inset (c, f, i). Note: AFM scanning area is 4 μm × 4 μm.

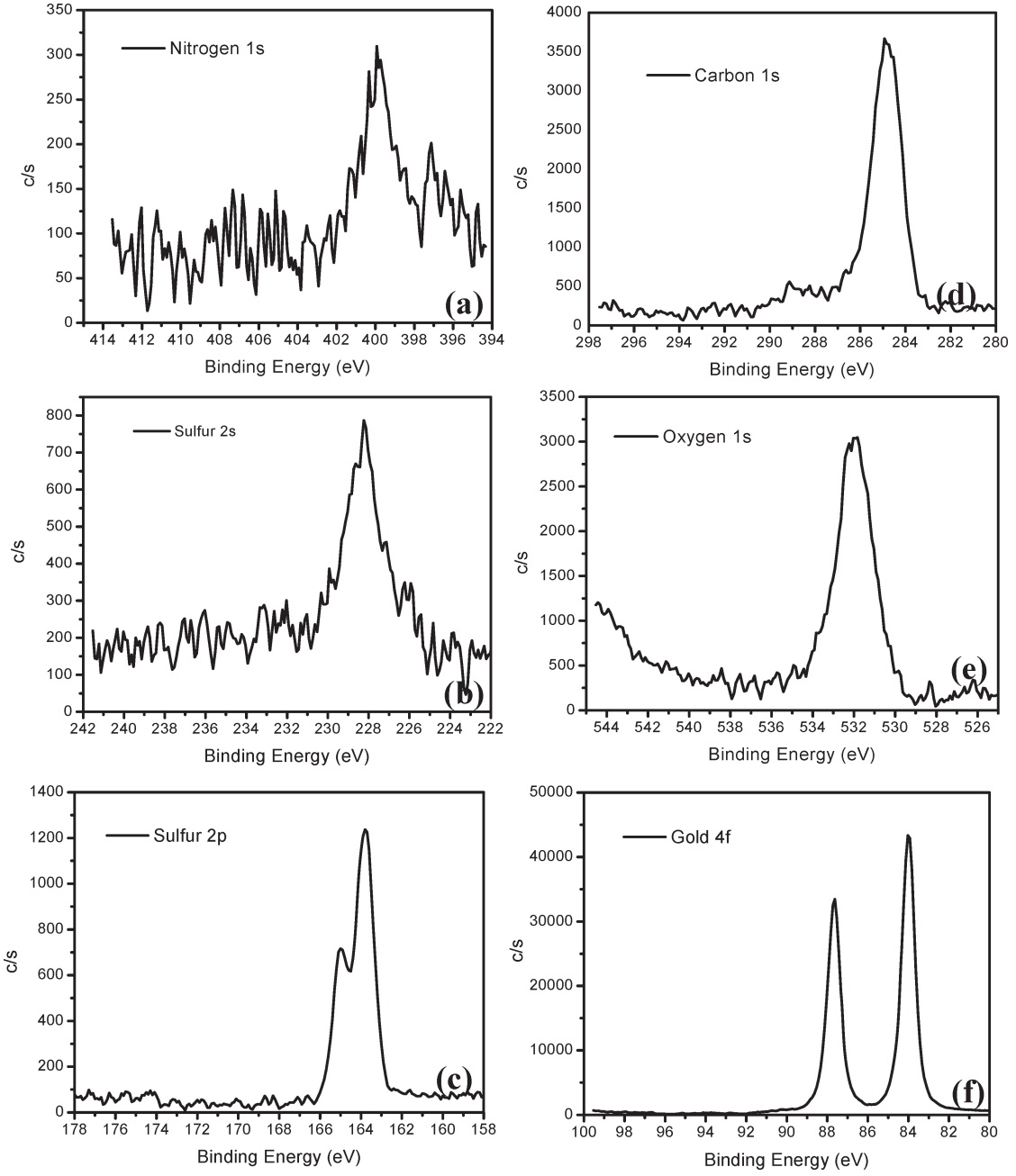

Figure 5. XPS high-resolutions scan of the MIP film showing different peaks: nitrogen (N) 1s (a), carbon (C) 1s (b), oxygen (O) 1s (c), sulfur (S) 2s (d), and sulfur (S) 2p (d).

After subjecting the E-MIP film to potential-induced washing, its topography image changed (Figure 4g compared to Figure 4d), which is more evident in the phase image (Figure 4i compared to Figure 4f). The E-MIP film appeared to be swollen as characterized by the slight increase in size of the features on the surface. This observation is confirmed by the values of the x and y scales in the line profile measurements after the constant potential washing. The x and y scales had increased by $\sim$0.07 μm and $\sim$3.5 nm, respectively. Furthermore, ellipsometry measurements verified the decrease in thickness of the polymer film, and the contact angle also decreased becoming slightly hydrophilic (Table 1) which is essential for the rebinding of the template that is in aqueous media. Thus, cavities of the guest molecule, a vital component as a sensor recognition element, were formed by carefully releasing the template from the polymer network. As an additional evidence on the successful removal of the imprinted molecule, the root-mean-square (rms) roughness (Figure 4a−c) of the three films was calculated, and their values were shown to be comparable to the rms values of the E-MIP films created by electropolymerization of a bis(bithiophene) monomer derivative.[21] Prior to removal of the template, the rms of the imprinted film is closer to the NIP film. After releasing the template from the highly cross-linked E-MIP film, the rms had increased, thus indicating a more porous film was created as a result of the formation of template cavities.

High-resolution XPS was performed with the E-MIP film to clearly validate the electropolymerization of the monomer and the entrapment of the template (Figure 5) and later on the removal of the imprinted template (Figure 7 in the Supporting Information). The appearance of the peak for S 2s at $\sim$228.2 eV (Figure 5b) and S 2p doublet peak between 163.0 and 166.0 eV (Figure 5c) confirmed the formation of the polymer film.

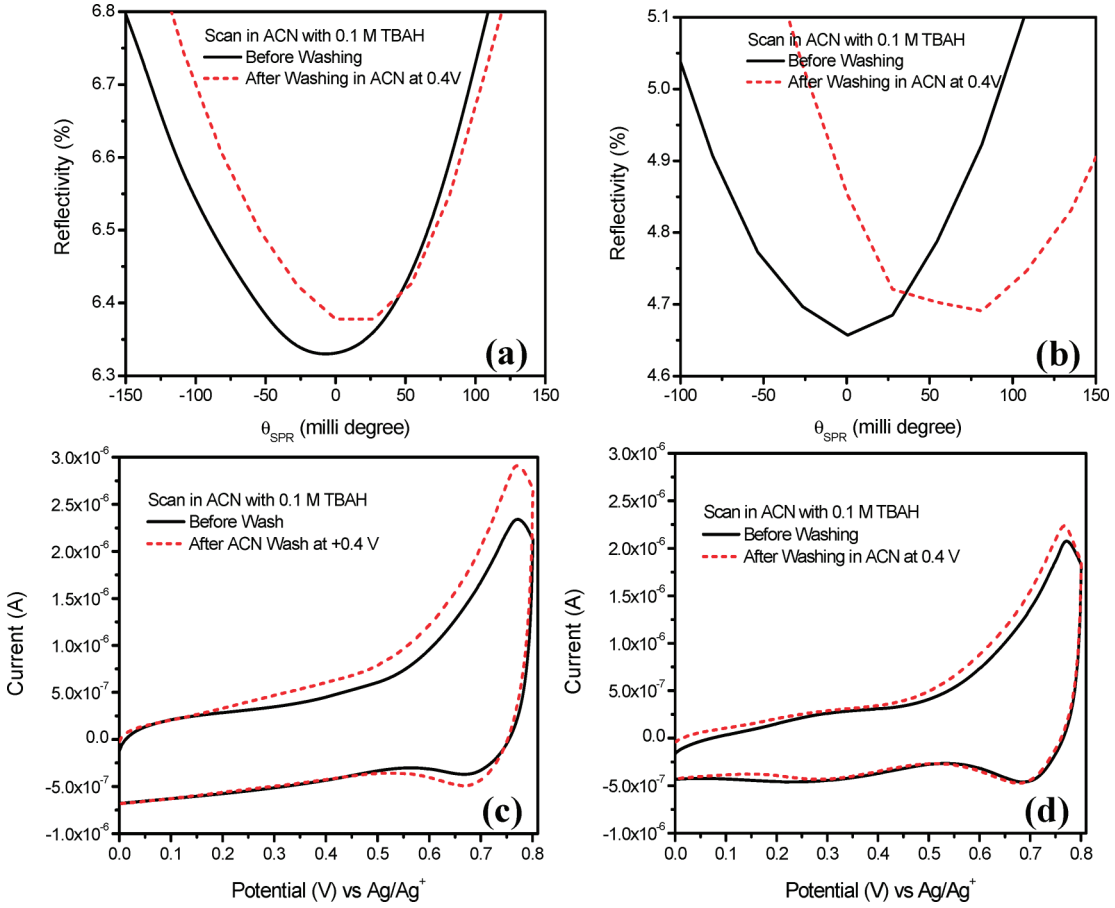

Figure 6. SPR angular scan of (a) MIP and (b) NIP. CV curve of (c) MIP and (d) NIP before and after washing of the template at constant potential in acetonitrile.

The doublet S 2p peak has been reported as a chemisorbed thiophene.[27] The peak at ~400.0 eV with a small peak shoulder at ~397.3 eV (Figure 5a) indicates the presence of N 1s, which is attributed to the nitrogen atoms in the heterocyclic ring of theophylline. This result verified the noncovalent immobilization of theophylline onto the poly-(terthiophene). The nitrogen element is a unique elemental marker of the template molecule, which is not present in the poly(terthiophene) film. The N 1s spectrum resembled that of the theophylline-modified surface, which contains two shouldering peaks due to the presence of two types of nitrogen functionalities (N1, 8 and N3, 5) in the structure of theophylline.[28] Moreover, earlier studies reported that the N 1s peaks located at the range between 400.0 and 400.5 eV were due to the H-bonding interactions of tertiary amine nitrogen and amide nitrogen atoms.[29] The other elements on the surface (Figure 5d,e) such as C 1s (between 283. 0 and 291.0 eV) and O 1s (between 529.0 and 537.0 eV) divulge the successful modification of the Au surface with the MIP film.[35,37] The appearance of the Au doublet peak between 83.0 and 89.0 eV (Figure 5f) confirmed that a thin and porous MIP film was fabricated on Au substrate.

Removal of the Template Guest Molecule: Importance of Constant Potential Washing. Following the MIP electropolymerization is the removal of the guest molecule, which was carried out to create an imprinted site. The efficiency of template removal from the highly cross-linked polymer film is very crucial to MIP film sensing. Moreover, upon removal of the template, the integrity of the cavities with its memory about the size, shape, and orientation of the chemical template functionality needs to be maintained. The inability to satisfy these important conditions would result in poor selectivity, limited sensitivity, and lack of stability of the MIP sensors. In order to overcome these challenges, thinner films of nanoscale thickness were used to enable easy removal of the template and to avoid deep burial of binding sites. AFM analysis showed the advantage of a thin film over a thick film. With a thicker polymer film (~50 nm), the AFM image demonstrates greater aggregations on its surface despite thorough washing with the solvent after electropolymerization (Figure 6 in the Supporting Information). Aside from making thin MIP films, the choice of appropriate solvents for template removal was also investigated. Sensing responses were compared for several solvents during the rebinding of the analyte (results not shown here) after solvent washing (in flow system). Acetonitrile, which can dissolve theophylline completely but not the poly(terthiophene), gave the highest sensing response compared to other solvents. Additionally, during the washing of the template with the best solvent (acetonitrile), a constant potential (0.4 V) was applied to dope (oxidize) the polymer film. The selected voltage was determined from the highest sensing response of the MIP film when different potentials were applied to it during washing.

In Figure 6a,b, the distinct shift in the SPR minimum relative to the curve before applying a constant potential can be attributed to (1) the change in thickness due to swelling and (2) the change in optical property (refractive index) resulting from the increase in conductivity of the polymer film. Unlike thicker films (greater than 0.5 μm), the change in the SPR minimum was caused only by the change in refractive index.[30]

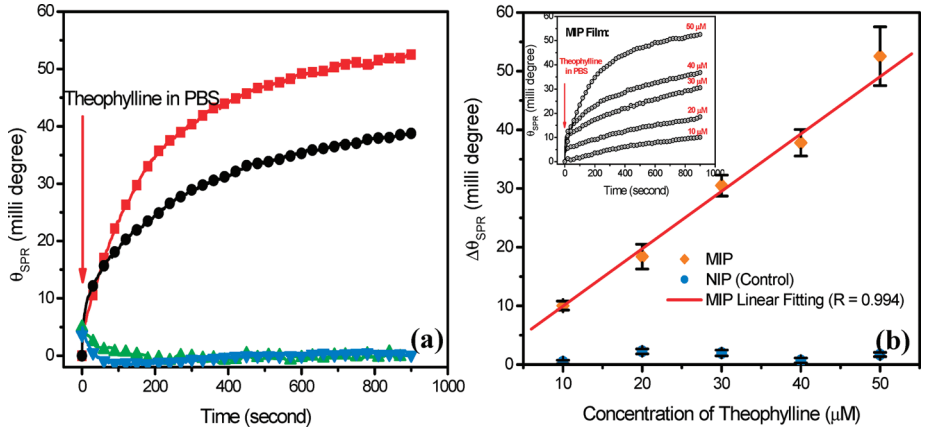

Figure 7. (a) *In situ* SPR sensing of theophylline (50 μM) using MIP film after ACN wash at 0.4 V (●), MIP film after ACN wash only (●), NIP film (▼), and bare gold (▲). (b) Calibration curve (each point taken at 900 s, raw data on inset) for theophylline using MIP (◆) vs NIP film (●). Buffer shift and bulk response were subtracted from the original sensogram.

Note that previously the doping process of thiophene-based polymers has been reported to create charges within the polymer network.[31] With charging, an electrostatic repulsion between the charges may occur, resulting in swelling of the polythiophene film. This facilitates the release of more template molecules, creating cavities for a sensor recognition element. In order to confirm the swelling of the imprinted polymer, the same experiment was performed with the NIP film (control), which showed a similar increase in the SPR minimum. Upon comparison, the E-MIP exhibited less angular change (about 20−40 mdeg) versus the NIP film (about 70−80 mdeg). This result can be due to the angular shift of the E-MIP through a combination of refractive index decrease (as a result of the formation of cavities or pores) and thickness increase of the polymer film due to swelling. The latter might be a more dominant effect, causing the SPR curve to shift further to higher angular minima values. In addition, the E-MIP film will have less swelling due to the imprinted templates entrapped inside the highly cross-linked polymer network.

By applying a constant positive potential (doping), the conductivity of the conjugated polymers will change accordingly. Conductivity is largest for the doped state and decreases for the dedoped state.[18] The increase in conductivity of the polymer film changes the imaginary part of the dielectric constant (eq 3). As a consequence, the SPR minimum will change in terms of width (angular) and depth (peak reflectivity) after applying a constant potential. A very similar trend about the SPR minimum shift was observed with a polypyrrole film after oxidation (doping).[10d] The dashed lines in Figure 6a,b are for 0.4 V corresponding to the doped (charge) state while the solid lines are for 0 V corresponding the dedoped (neutral) state of poly(terthiophene).

To further investigate poly(terthiophene) doping and the release of theophylline, CV electrochemical experiments were utilized. From the CV scan, both films (MIP and NIP) showed an increase in current at the oxidation peak regime (~0.6−0.8 V) after applying a constant positive potential during washing. This result indicates an increase in conductivity of the polymer films, validating the doping process. Interestingly, the E-MIP had a higher current increase compared to the NIP film. This can be attributed to the diffusion of more redox probe (PF_6^-) into the doped polymer film as a result of the formation of more pores within the MIP. Previously, the creation of porous MIP film after solvent extraction was determined by the insertion of more redox probe as monitored by an electrochemistry technique.[21] Nevertheless, the peak potentials of both NIP and E-MIP films remained the same, proving the stability of the poly(terthiophene) against the washing steps.

The various characterization techniques employed reveal evidence of the release of the template molecule from the polymer film. In order to confirm the results, an XPS high-resolution scan was performed with the MIP film to determine approximately the quantitative amount of template molecules that were removed during the constant potential washing. Results showed that the N 1s peak from the theophylline had decreased by about 87% (Figure 7a in the Supporting Information). This observation suggested an efficient removal of the template was achieved. Moreover, the S 2s peak area, which is only due to poly(terthiophene), remained almost constant, verifying the stability of the polymer film even with the potential induced washing (Figure 7b in the Supporting Information). The constant potential washing enabled the fast and effective removal of imprinted molecules for only 10 min, much faster than the earlier methods that took hours and used a harsh solvent condition (i.e., acids or bases) for template extraction.[12,31] With a mild solvent condition that we applied for washing, the integrity of the imprinted cavities that serve as the recognition element of the MIP sensor is well maintained.

Performance of the SPR Sensor Platform. The MIP film activity was evaluated by sensing of the template using *in situ* SPR measurements.[33] In terms of analyte detection, SPR offers a direct and efficient method over other analytical techniques. Currently, the measurement of theophylline is carried out regularly in many clinical laboratories using gas/liquid chromatography methods and commercial immunoassays, all of which are relatively tedious and time-consuming as compared to SPR detection.[1a,b] Figure 7a illustrates the kinetic profile of the rebinding of theophylline onto different substrates from a 50 μM solution. The E-MIP film shows a good sensing response creating a shift in the SPR angle of up to ~40 mdeg. The same MIP film was used for other sensing experiments after washing the bound analyte with application of a constant potential of 0.4 V in acetonitrile. An equivalent amount of time was used when the E-MIP film was washed with acetonitrile without applying a constant potential. A change in the SPR angle of about 50 mdeg was observed after the rebinding of the template. Compared to solvent washing alone, a ~30% increase in the SPR response was observed from the E-MIP film after constant potential washing in acetonitrile was applied. This result supported our claim that by applying a constant

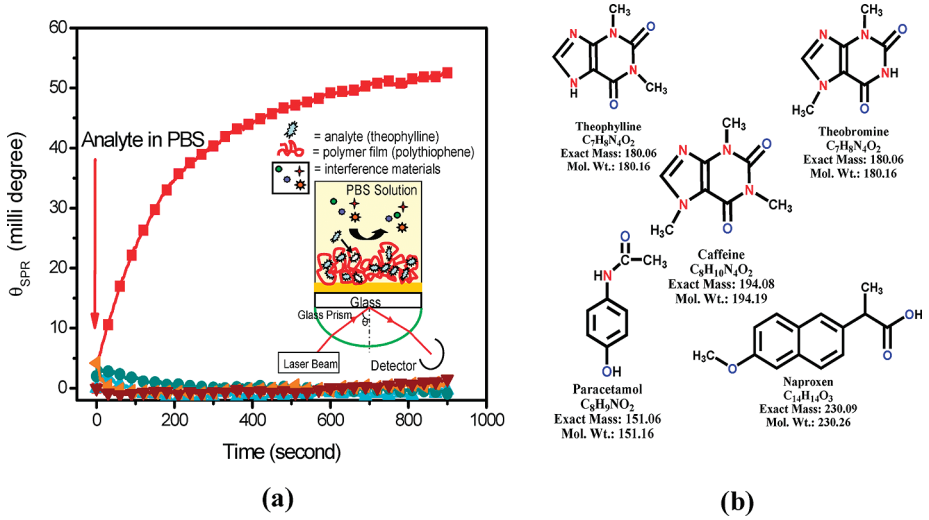

Figure 8. (a) Selectivity study of the MIP sensor film using *in situ* SPR sensing of theophylline, 50 μM (■) versus different analytes: theobromine, 500 μM (●); caffeine, 500 μM (▲); paracetamol, 50 μM (▼); and naproxen, 50 μM (tilted ▲). Note: buffer shift and bulk response were subtracted from the original sensogram. (b) Chemical structure of the compounds used for selectivity study.

potential at 0.4 V during washing more guest molecules are removed from the polymer network, therefore creating more imprinted sites for template sensing. Two control experiments were also performed to compare with the sensing response of the MIP film: adsorption of 50 μM theophylline (1) onto NIP film and (2) on bare gold. It is evident that there is no observable change in the SPR angle during the adsorption of theophylline on these substrates. These data proved that the sensing of theophylline observed in the MIP film was mainly due to the formation of cavities or imprinted sites, which served as the selective sensor recognition element for the MIP film. Moreover, the improved sensing of the imprinted template by the MIP film was further confirmed by imprinting other drug molecules such as paracetamol and naproxen using exactly the same monomer and fabrication procedure. Likewise, a higher sensing response was observed with the MIP films that were subjected to potential-induced washing at 0.4 V (Figure 8 in the Supporting Information).

Sensitivity Study. To determine the sensitivity of the fabricated MIP film, a calibration study was performed by injecting different concentrations of the templates (Figure 7b). This experiment was also performed using the NIP film (control) (Figure 9 in the Supporting Information), which showed no observable response as compared to the MIP film. The slight increase in the SPR angle is due to nonspecific binding of the theophylline onto the NIP film. The concentration of interest to detect theophylline is within the 10−50 μM dynamic range which corroborates a recent work regarding the detection of theophylline using RNA-aptamer.[34] The calibration plot (Figure 7b) showed a linearity in the range 10−50 μM concentrations of theophylline with a correlation coefficient (R) of 0.994. The sensitivity of the MIP SPR sensor was determined from the slope of the calibration curve[36,36] and was equivalent to 1.044 mdeg μM^{-1}. The limit of detection (LOD, equal to $3\sigma m^{-1}$) and limit of quantification (LOQ, equal to $10\sigma m^{-1}$) of determining theophylline were 3.362 and 11.207 μM, respectively, where σ is the standard deviation and m is the slope of the calibration plot.[37] Finally, the sensogram curves were evaluated by numerical integration algorithm (OriginLab, version 7) of nonlinear curve fitting using monomolecular growth model to calculate for the association rate constant (k_a).[38] The calculated observed rate constant (k_{obs}) in the association phase was plotted against the concentration of theophylline to determine k_a from the resulting straight line using linear regression (Figure 10 in the Supporting Information) where the calculated k_a value is equivalent to 82.1 M^{-1} s^{-1}.

Selectivity Study. Selectivity is the ability of the sensor to discriminate between different analytes. Thus, in order to test the binding selectivity of the MIP film, a sensing experiment was conducted using different but structurally analogous compounds (also called interference compounds or analogues). Finding a sensor that will respond to only one analyte is ideal. However, it is more typical to find a sensor that will respond primarily to one analyte with limited responses to other similar analytes.[39] This sensor platform showed a high selectivity during real-time sensing of closely related analytes such as caffeine and theobromine. Theobromine and theophylline have identical molecular weights (180.06 g/mol). The only difference between theobromine to the target analyte is the substitution of 5-N with a methyl group instead of the 8-N position (Figure 8b). Moreover, caffeine, theobromine, and theophylline are closely related compounds by a metabolic process occurring in the liver.[40] At present, clinical laboratories that employ gas/liquid chromatography and commercial immunoassay in detecting theophylline are experiencing interfering responses from caffeine and theobromine,[1a,b] hence resulting in an inaccurate measurement of theophylline concentration. In addition to these two analytes, paracetamol and naproxen were also used to distinguish the selectivity of the MIP sensor. From Figure 8a, it is observed that the MIP film did not show any observable response upon exposure to theobromine (500 μM) and caffeine (500 μM) albeit the concentration is 10 times greater than theophylline (50 μM), which showed a ~50 mdeg change. Similarly, the MIP film did not demonstrate a noticeable response for paracetamol and naproxen, making the fabricated MIP film highly selective to only the template molecule. To better express the effect of the interference compounds, the interference ratio (IR) is determined.[41] It is calculated by taking the ratio of the SPR angular change in the E-MIP film upon binding the interference compounds to the SPR angular change due to the binding of theophylline ($IR = \Delta\theta_{SPR,analogue}/\Delta\theta_{SPR,theophylline}$). A lower IR value ($\ll 1$) denotes very less or minimal interaction between the E-MIP film and the analogue, whereas a value of 1 means a complete binding. The IR of the theobromine and caffeine (with concentration 10-fold higher than theophylline) are both equal to 0.02, which means that the E-MIP film has very less affinity to these compounds. To verify the high selectivity of the E-MIP

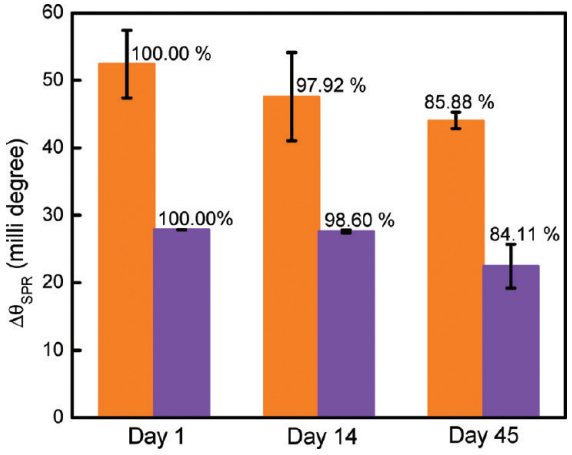

Figure 9. Stability study of the MIP film: Injection of 50 μM (orange bar graph) and 35 μM (violet bar graph) concentration of theophylline.

film, other drug molecules (i.e., paracetamol and naproxen) were also imprinted using the same functional and cross-linking monomer (G0-3T COOH), and the fabricated E-MIPs were subjected to different compounds with some of them closely resembling the structure of the template molecule. The results are summarized in Figure 11 of the Supporting Information. Similarly, the other E-MIP films demonstrated a high selectivity toward the imprinted drug molecule and only a limited response to other compounds due to nonspecific binding. The outstanding selectivity of the E-MIP is attributed to the robust imprinted sites or cavities of the polymer film that retained precisely the memory of the size, shape, and orientation of chemical functionality of the template molecule theophylline.

Stability Study. The working lifetime of the MIP sensor film was evaluated by performing a stability study (Figure 9). This study measures the ability of the sensor in maintaining its sensing performance over a certain period of time. Briefly, the experiment was carried out by injecting 35 and 50 μM concentration of the template onto the MIP film and then monitoring the SPR response as a result of the *in situ* analyte binding. Two concentrations were selected to confirm the result. Also, this experiment was repeated on different areas of the same substrate that was kept under dry and ambient conditions for 14 and 45 days. After 14 days, the SPR response has decreased by ~2.08% and ~1.40% for 50 and 35 μM concentrations of theophylline, respectively, due to template binding. Moreover, after 45 days, the sensing response has decreased further to ~14.12% and ~15.89% for 50 and 35 μM concentrations of the template, respectively. Therefore, the fabricated MIP film does not only exhibit outstanding selectivity and high sensitivity but also very good stability, which can retain about 85% of its original response after 45 days of storage in dry and ambient conditions.

Conclusions

A facile protocol for making an E-MIP/SPR sensor device that is highly sensitive and selective to the target analyte has been demonstrated using polyterthiophene. Unlike most MIP systems, the E-MIP sensor device uses an electropolymerization−cross-linking procedure with a template−monomer complex for molecular recognition, providing a binding functionality to a future analyte molecule. The theoretical modeling studies by Spartan (AM1, semiempirical calculations) highlighted the interactions between the functional monomer and the template (prepolymerization complex), forming an energetically stable cross-linkable conformation. The use of an electrostatic induced washing highlighted a more efficient and rapid way of removing the guest molecule from the highly cross-linked polymer film. With the versatility of the molecular imprinting technique combined with electropolymerization, the E-MIP should be a promising approach to the fabrication of ultrathin sensor films that can be easily attached to various electrode transducers other than SPR. This work has a potential not only for the fabrication of a sensor film that would detect theophylline but also for distinguishing other important analytes from their more closely related molecular structures in separation procedures.

Acknowledgment. The authors acknowledge funding from NSF ARRA CBET-0854979, DMR-10-06776, CHE-1041300, and Robert A Welch Foundation, E-1551. The authors also acknowledge the Brinkmann-Eco Chemie (Metro Ohm USA) for technical support on the potentiostat−SPR setup and providing the gold disk for the SPR measurements. We also acknowledge technical support from Agilent Technologies and Optrel GmBH.

Supporting Information Available: Details of the synthesis of monomer and the corresponding NMR spectra, 2D computer generated images of the other monomer-to-template ratios calculated by Spartan, CV electropolymerization and AFM images of NIP, XPS spectra before and after template removal, SPR binding kinetic curves, and curve fitting of the SPR kinetic curve. This material is available free of charge via the Internet at http://pubs.acs.org.

References and Notes

(1) (a) Kawa, M.; Kato, M. *Methods Find. Exp. Clin. Pharmacol.* **2000**, *22*, 309–320. (b) Rowe, D. J.; Watson, I. D.; Williams, J.; Berry, D. J. *Ann. Clin. Biochem.* **1988**, *25*, 4–26. (c) Howard, C. E.; Capers, C. C.; Bess, D. T.; Anderson, R. J. *Am. J. Hosp. Pharm.* **1994**, *51*, 1672. (d) Herrmann, G.; Aynesworth, M. B.; Martin, J. *J. Lab. Clin. Med.* **1937**, *23*, 135–148.

(2) Thomas, J. B.; Yen, J. H.; Schantz, M. M.; Porter, B. J.; Sharpless, K. E. *J. Agric. Food Chem.* **2004**, *52*, 3259–3263.

(3) (a) Arshady, R.; Mosbach, K. *Macromol. Chem. Phys.* **1981**, *182*, 687–692. (b) Vlatakis, G.; Andersson, L. I.; Muller, R.; Mosbach, K. *Nature* **1993**, *361*, 645–647.

(4) (a) Hart, B. R.; Rush, D. J.; Shea, K. J. *J. Am. Chem. Soc.* **2000**, *122*, 460–465. (b) Matsui, J.; Miyoshi, Y.; Doblhoff-Dier, O.; Takeuchi, T. *Anal. Chem.* **1995**, *67*, 4404–4408. (c) Ferrer, I.; Lanza, F.; Tolokan, A.; Horvath, V.; Sellergren, B.; Horvai, G.; Barcelo, D. *Anal. Chem.* **2000**, *72*, 3934–3941. (d) Piletsky, S. A.; Karim, K.; Piletska, E. V.; Day, C. J.; Freebairn, K. W.; Legge, C.; Turner, A. P. F. *Analyst* **2001**, *126*, 1826–1830.

(5) (a) Turner, N. W.; Liu, X.; Piletsky, S. A.; Hlady, V.; Britt, D. W. *Biomacromolecules* **2007**, *8*, 2781–2787. (b) Mayuko Tatemichi, M.; Sakamoto, M.; Mizuhata, M.; Deki, S.; Takeuchi, T. *J. Am. Chem. Soc.* **2007**, *129* (135), 10906–10910.

(6) (a) Kang, X.; Jin, Y.; Cheng, G.; Dong, S. *Langmuir* **2002**, *18*, 1713–1718. (b) Bailey, L. E.; Kambhampati, D.; Kanazawa, K. K.; Knoll, W.; Frank, C. W. *Langmuir* **2002**, *18*, 479–489.

(7) (a) Baba, A.; Taranekar, P.; Ponnapati, R. R.; Knoll, W.; Advincula, R. C. *ACS Appl. Mater. Interfaces*, Articles ASAP. (b) Kaewtong, C.; Jiang, G.; Park, Y.; Fulghum, T.; Baba, A.; Pulpoka, P.; Advincula, R. C. *Chem. Mater.* **2008**, *20*, 4915–4924.

(8) Taranekar, P.; Baba, A.; Park, J. Y.; Fulghum, T.; Advincula, R. *Adv. Funct. Mater.* **2006**, *16*, 2000–2007.

(9) Knoll, W. *Annu. Rev. Phys. Chem.* **1998**, *49*, 569–638.

(10) (a) Baba, A.; Lubben, J.; Tamada, K.; Knoll, W. *Langmuir* **2003**, *19*, 9058–9064. (b) Baba, A.; Knoll, W. *J. Phys. Chem. B* **2003**, *107*, 7733–7738. (c) Schweiss, R.; Lubben, J.; Johannsmann, D.; Knoll, W. *Electrochim. Acta* **2005**, *50*, 2849–2856. (d) Damos, F. S.; Luz, R. C. S.; Kubota, L. T. *Electrochim. Acta* **2006**, *51*, 1304–1312.

(11) (a) Baba, A.; Advincula, R.; Knoll, W. *J. Phys. Chem. B* **2002**, *106*, 1581–1587. (b) Baba, A.; Knoll, W.; Advincula, R. *Rev. Sci. Instrum.* **2006**, *77*, 064101−1–064101−6. (c) Ravindranath, R.; Ajikumar, P.; Baba, A.; Bahuleyan, S.; Hanafiah, N.; Advincula, R.; Knoll, W.; Valiyaveettil, S. *J. Phys. Chem. B* **2007**, *111*, 6336–6343. (d) Baba, A.; Onishi, K.; Knoll, W.; Advincula, R. *J. Phys. Chem. B* **2004**, *108*,

18949–18955. (e) Baba, A.; Tian, S.; Stefani, F.; Xia, C.; Wang, Z.; Advincula, R.; Johannsmann, D.; Knoll, W. *J. Electroanal. Chem.* **2004**, *562*, 95–103. (f) Baba, A.; Park, M.-K.; Advincula, R.; Knoll, W. *Langmuir* **2002**, *18* (12), 4648–4652. (g) Xia, C.; Advincula, R. *Langmuir* **2002**, *18* (9), 3555–3560.
(12) Ulyanova, Y. V.; Blackwell, A. E.; Minteer, S. D. *Analyst* **2006**, *131*, 257–261.
(13) Taranekar, P.; Fulghum, T.; Baba, A.; Patton, D.; Advincula, R. *Langmuir* **2007**, *23*, 908–917.
(14) Batra, D.; Shea, K. J. *Curr. Opin. Chem. Biol.* **2003**, *7*, 434–442.
(15) Sauerbrey, G. *Z. Phys.* **1959**, *155*, 206–222.
(16) Bethencourt, M. I.; Srisombat, L.; Chinwangso, P.; Lee, T. R. *Langmuir* **2009**, *25*, 1265–1271.
(17) (a) Schwarz, L.; Bowyer, M. C.; Holdsworth, C. I.; McCluskey, A. *Aust. J. Chem.* **2006**, *59*, 129–134. (b) Holdsworth, C. I.; Bowyer, M. C.; Lennard, C. *Aust. J. Chem.* **2005**, *58*, 315–320. (c) Schwarz, L.; Holdsworth, C. I.; McCluskey, A.; Bowyer, M. C. *Aust. J. Chem.* **2004**, *57*, 759–764.
(18) Georgiadis, R.; Peterlinz, K. A.; Rahn, J. R.; Peterson, A. W.; Grassi, J. H. *Langmuir* **2000**, *16* (17), 6759–6762.
(19) (a) Dong, H.; Cao, X.; Li, C. M.; Hu, W. *Biosens. Bioelectron.* **2008**, *23*, 1055–1062. (b) Hu, W.; Li, C. M.; Cui, X.; Dong, H.; Zhou, Q. *Langmuir* **2007**, *23*, 2761–2767. (c) Chegel, V.; Raitman, O.; Katz, E.; Gabai, R.; Willner, I. *Chem. Commun.* **2001**, 883–884.
(20) Fulghum, T.; Abdul Karim, S, M.; Baba, A.; Taranekar, P.; Nakai, T.; Masuda, T.; Advincula, R. C. *Macromolecules* **2006**, *39*, 1467–1473. (b) Patton, D.; Taranekar, P.; Fulghum, T.; Advincula, R. C. *Macromolecules* **2008**, *41*, 6703–6713. (c) Taranekar, P.; Fulghum, T.; Patton, D.; Ponnapati, R.; Clyde, G.; Advincula, R. C. *J. Am. Chem. Soc.* **2007**, *129*, 12537–12548.
(21) Pietrzyk, A.; Kutner, W.; Chitta, R.; Zandler, M. E.; D'Souza, F.; Sannicolo, F.; Mussini, P. R. *Anal. Chem.* **2009**, *81*, 10061–10070.
(22) Kossmehl, G.; Fechler, D.; Plieth, W.; Zhang, W. F.; Zerbino, J. *DECHEMA Monogr.* **1990**, *121*, 279.
(23) Rasch, B.; Vielstich, W. *J. Electroanal. Chem.* **1994**, *370*, 109–117.
(24) Roncali, J. *Chem. Rev.* **1992**, *92*, 711–738.
(25) (a) Mathieu, S.; Trinquier, G. *Phys. Chem. Chem. Phys.* **2009**, *11*, 8183–8190. (b) Khan, F. L. A.; Sivagurunathan, P. *Phys. Chem. Liq.* **2008**, *46*, 504–509. (c) Sibrian-Vazquez, M.; Spivak, D. A. *J. Am. Chem. Soc.* **2004**, *126*, 7827–7833.
(26) (a) Kobayashi, T.; Fukaya, T.; Abe, M.; Fujii, N. *Langmuir* **2002**, *18*, 2866–287. (b) Han, M.; Kane, R.; Goto, M.; Belfort, G. *Macromolecules* **2003**, *36*, 4472–4477.
(27) (a) Rodriguez, J. A.; Dvorak, J.; Jirsak., T. *Surf. Sci.* **2000**, *457*, L413–L420. (b) Liu, G.; Rodriguez, J. A.; Dvorak, J.; Hrbek, J.; Jirsak, T. *Surf. Sci.* **2002**, *505*, 295–307.
(28) Kuijpens, J. M. H.; Kardaum, G. A.; Blezer, R.; Pijpers, A. P.; Koole, L. H. *J. Am. Chem. Soc.* **1995**, *117* (34), 8691–8697.
(29) (a) Luo, X.; Goh, S. H.; Lee, S. Y.; Tan, K. L. *Macromolecules* **1998**, *31*, 3251–3254. (b) Liu, Y.; Goh, S. H.; Lee, S. Y.; Huan, C. H. A. *Macromolecules* **1999**, *32*, 1967–1971. (c) Zhou, X.; Goh, S. H.; Lee, S. Y.; Tan, K. L. *Polymer* **1998**, *39*, 3631–3640. (d) Zhou, X.; Goh, S. H.; Lee, S. Y.; Tan, K. L. *Appl. Surf. Sci.* **1997**, *119*, 60–66.
(30) Kuckling, D.; Harmon, M. E.; Frank, C. W. *Macromolecules* **2002**, *35*, 6377–6383.
(31) (a) Schopf, G.; Kossmehl, G. *Adv. Polym. Sci.* **1997**, 80. (b) Kossmehl, G.; Kabbeck-Kupijai, D.; Niemitz, M. *Chiuz.* **1990**, *24*, 106. (c) Niemitz, M.; Kossmehl, G. *Angew. Makromol. Chem.* **1991**, *185*−*186*, 147. (d) Kossmehl, G.; Niemitz, M. *Synth. Met.* **1991**, *41*, 1065–1071.
(32) (a) Niu, J.; Liu, Z.; Fu, L.; Shi, F.; Ma, H.; Ozaki, Y.; Zhang, X. *Langmuir* **2008**, *24*, 11988–11994. (b) Ersoz, A.; Diltemiz, S. E.; Ozcan, A. A.; Denizli, A.; Say, R. *Biosens. Bioelectron.* **2008**, *24*, 742–747. (c) Gong, J.-L.; Gong, F.-C.; Kuang, Y.; Zeng, G.-M.; Shen, G.-L.; Yu, R.-Q. *Anal. Bioanal. Chem.* **2004**, *379*, 302–307. (d) Tan, Y.; Zhou, Z.; Wang, P.; Nie, L.; Yao, S. *Talanta* **2001**, *55*, 337–347. (e) Weetall, H.; Rogers, K. R. *Talanta* **2004**, *62*, 329–335. (f) Yan, H.; Row, K. H.; Yang, G. *Talanta* **2008**, *75*, 227–232.
(33) (a) Bolduc, O. R.; Masson, J.-F. *Langmuir* **2008**, *24*, 12085–12091. (b) Hyoungwon Baac, H.; Hajos, J. P.; Lee, J.; Kim, D.; Kim, S. J.; Shuler, M. L. *Biotechnol. Bioeng.* **2006**, *94* (4), 815–819. (c) Siegers, C.; Biesalski, M.; Haag, R. *Chem.—Eur. J.* **2004**, *10*, 2831–2838.
(34) (a) Ferapontova, E. E.; Olsen, E. M.; Gothelf, K. V. *J. Am. Chem. Soc.* **2008**, *130*, 4256–4258. (b) Ferapontova, E. E.; Shipovskov, S.; Gorton, L. *Biosens. Bioelectron.* **2007**, *22*, 2508–2515.
(35) Syu, M.-J.; Chiu, T.-C.; Lai, C.-Y.; Chang, Y. S. *Biosens. Bioelectron.* **2006**, 550–557.
(36) (a) Rudy, J. L.. *Clin. Chem.* **1989**, *35*, 509. (b) Cha, W.; Tung, W.-C.; Meyerhoff, M. E.; Takayama, S. *Anal. Chem.* **2010**, *82*, 3300–3305.
(37) (a) Adhoum, N.; Monser, L.; Toumi, M.; Boujlel, K. *Anal. Chim. Acta* **2003**, *495*, 69–75. (b) Hasebe, K.; Osteryoung, J. *Anal. Chem.* **1975**, *47*, 2412–2418.
(38) Gronewold, T. M. A.; Antje Baumgartner, A.; Weckmann, A.; Knekties, J.; Egler, C. *Acta Biomater.* **2009**, *5*, 794–800.
(39) (a) Bui, B. T. S.; Belmont, A.-S.; Witters, H.; Haupt, K. *Anal. Bioanal. Chem.* **2008**, *390*, 2081–2088. (b) Gomez-Caballero, A.; Goicolea, A.; Barrio, R. J. *Analyst* **2005**, *130*, 1012–1018. (c) Yang, M.-L.; Li, Y.-Z. *Anal. Lett.* **2004**, *37* (10), 2043–2052.
(40) The Pharmacogenetics and Pharmacogenomics Knowledge Base. Retrieved on 2006-08-14.
(41) Mazzotta, E.; Picca, R. A.; Malitesta, C.; Piletsky, S. A.; Piletska, E. V. *Biosens. Bioelectron.* **2008**, *23*, 1152–1156.